

Collective Dynamics of Bose–Einstein Condensates in Optical Cavities

J. Keeling, M. J. Bhaseen, and B. D. Simons

University of Cambridge, Cavendish Laboratory, Cambridge, CB3 0HE, UK.

(Dated: November 9, 2018)

Recent experiments on Bose–Einstein condensates in optical cavities have observed a coherent state of the matter–light system — superradiance. The nature of these experiments demands consideration of collective dynamics. Including cavity leakage and the back-reaction of the cavity field on the condensate, we find a rich phase diagram including a variety of multi-phase co-existence regions, and a regime of persistent optomechanical oscillations. Proximity to some of the phase boundaries results in critical slowing down of the decay of many-body oscillations, which can be enhanced by large cavity loss.

PACS numbers: 37.30.+i, 42.50.Pq

The tremendous advances in preparing Bose–Einstein condensates (BEC) in optical cavities have opened new frontiers combining cold atoms and quantum optics. It is now possible to enter the strongly coupled regime of cavity quantum electrodynamics (QED) [1, 2] in which atoms exchange photons many times before spontaneous emission and cavity losses set in. The inherent cavity leakage also provides a valuable window on these quantum many-body systems. In particular, it allows for *in situ* non-demolition measurements of condensate properties via optical transmission [3, 4]. The strong matter–light coupling also supports collective dynamics and back-reaction effects, stimulating new directions in cavity optomechanics [5, 6] and self-organised atomic ensembles [7–13].

More recently, these capabilities have been elevated through observation of the superradiance transition in BECs [14, 15]. The atom mediated coupling between a transverse pump field and a cavity mode leads to a realisation of the Dicke model [16–19], in which atomic momenta play the role of spin states; see Fig. 1. A significant merit of this approach is that the energy splitting of the two-level systems is small enough so that the Dicke superradiance transition may be realised with light at optical frequencies [14, 15]. These experiments are a landmark in the study of quantum phase transitions involving spins, and offer exciting and unique prospects for exploring their static and dynamic properties. Indeed, the time-dependent nature of these measurements demands consideration of collective dynamics.

Motivated by these developments we investigate the collective dynamics of BECs in optical cavities. Our two primary goals are to establish the generic behaviour, and to focus on the precise experimental realisation in Ref. [15]. We obtain a surprisingly rich phase diagram for a broad range of parameters, and find distinct regimes of dynamical behaviour, including several regions of multi-phase co-existence, and regions of persistent optomechanical oscillations. For recent theoretical work see Ref. [20].

The experiments in Ref. [15] consist of a ^{87}Rb BEC

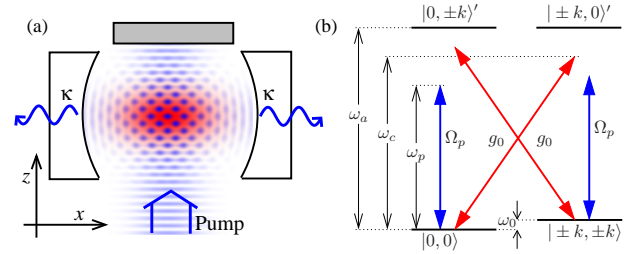


FIG. 1. Experimental setup [15]. (a) BEC in a transversely pumped cavity with pumping frequency, ω_p , and strength Ω_p , single-atom cavity coupling g_0 , atomic transition frequency ω_a , cavity frequency ω_c , and cavity decay rate, κ . (b) Energy levels and pumping scheme showing the two-level splitting, $\omega_0 = 2\omega_r$, in the effective Dicke model, where $\omega_r = k^2/2m$ is the recoil energy.

with $N \sim 10^5$ atoms in an optical cavity with a transverse pumping laser; see Fig. 1. The excited atoms may re-emit photons either along or transverse to the cavity axis. This process couples the zero momentum atomic ground state, $|p_x, p_z\rangle = |0, 0\rangle$, to the symmetric superpositions $|\pm k, \pm k\rangle$, with an additional photon momentum along the cavity or pump directions. This yields an effective two-level system or “spin”, where the splitting, ω_0 , is twice the atomic recoil energy, $\omega_r = k^2/2m$. One obtains an effective Dicke model for collective spins, \mathbf{S} , of length $N/2$, coupled to radiation ψ [14, 15]

$$H = \omega \psi^\dagger \psi + \omega_0 S_z + U S_z \psi^\dagger \psi + g(\psi^\dagger S^- + \psi S^+) + g'(\psi^\dagger S^+ + \psi S^-), \quad (1)$$

where, $\omega = \omega_c - \omega_p + NU_0(1 + \mathcal{M})/2$, $\omega_0 = 2\omega_r$, $U = U_0\mathcal{M}$, \mathcal{M} is a matrix element of order unity, and $U_0 = g_0^2/(\omega_p - \omega_a)$ encodes the back-reaction of the cavity light field on the BEC. The model includes both co-rotating and counter-rotating matter–light couplings, denoted g and g' . In the experiment $g = g' = g_0\Omega_p/(\omega_p - \omega_a)$ [15].

To describe the dynamics of the matter–light system

(1) we construct the Heisenberg equations of motion

$$\begin{aligned}\dot{S}^- &= -i(\omega_0 + U\psi^\dagger\psi)S^- + 2i(g\psi + g'\psi^\dagger)S_z, \\ \dot{S}_z &= -ig\psi S^+ + ig\psi^\dagger S^- + ig'\psi S^- - ig'\psi^\dagger S^+, \\ \dot{\psi} &= -[\kappa + i(\omega + US_z)]\psi - igS^- - ig'S^+, \end{aligned} \quad (2)$$

where $S^\pm \equiv S_x \pm iS_y$, κ is the cavity loss rate, and we neglect atom loss [15]. Various limits of these equations have been explored in different contexts. For $\kappa = g' = 0$ they describe fermionic pairing, where ψ is the Feshbach resonant closed state molecular field [21]. This regime also arises for polariton condensates and phase-locking of oscillators [22]. More recently, for $g = g'$, they have emerged in an elegant proposal for realising the Dicke model [14]. As we will see, solutions of the more general equations strongly influence $g = g'$ dynamics.

In order to anchor the complete phase diagram, we start with $U = 0$ and consider $U \neq 0$ below. Numerical solution of equations (2), and the arguments below, yield the rich phase diagram in Fig. 2, where the phases indicate stable attractors of the long time dynamics. Four distinct phases exist corresponding to all spins down and no photons (\Downarrow), all spins up and no photons (\Uparrow), a superradiant phase with photons (SR), and co-existence of the superradiant and down attractors; see S1-S4 in Fig. 2. Such co-existence, or bistability, is related to the observed optomechanical oscillations in a different system, where matter–light coupling is only through the back-reaction [5, 6, 23]. In spite of the cavity decay rate, κ , which may be large, the counter-rotating terms stabilise superradiant steady states. Indeed, dropping the derivatives in equation (2) renders algebraic equations, and the determinantal condition for non-trivial solutions ($\psi \neq 0$) yields

$$S_z = \frac{-\omega\omega_0(g^2 + g'^2) \pm \sqrt{(2\omega\omega_0gg')^2 - \omega_0^2\kappa^2(g^2 - g'^2)^2}}{2(g^2 - g'^2)^2}. \quad (3)$$

The conditions for real physical solutions yield the blue phase boundaries shown in Fig. 2 (a). Setting $S_z = -N/2$ in equation (3) yields the “upper” boundary shown in Fig. 2 (a) [24]. The vanishing of the square root yields the “lower” boundary, $g' = g\sqrt{\alpha_-/\alpha_+}$, where $\alpha_\pm = \sqrt{\omega^2 + \kappa^2} \pm \omega$, delineating the onset of co-existence. In order to identify the green phase boundary in Fig. 2 (a) it is necessary to consider the stability of the steady states. We consider fluctuations about an arbitrary configuration, $\mathbf{S} = \mathbf{S}_0 + \delta\mathbf{S}$, $\psi = \psi_0 + \delta\psi$, with frequency ν . Instability occurs if $\text{Im}(\nu) > 0$, and this yields the critical line $g' = g\sqrt{\beta_+/\beta_-}$ shown in Fig. 2 (a), where $\beta_\pm = (\omega \pm \omega_0)^2 + \kappa^2$. This separates the stable normal state \Downarrow from the stable inverted state \Uparrow . For the chosen parameters this gives $g'/g = 1.0043$, very close to unity. The dynamics at $g = g'$ may thus be strongly influenced by proximity to this phase boundary. The parameters used in Fig. 2 follow the hierarchy $\omega, \kappa \gg g\sqrt{N} \gg \omega_0$, in which

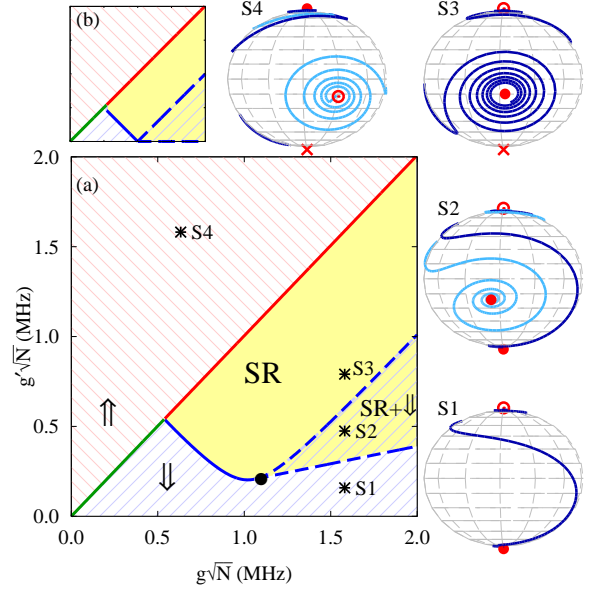


FIG. 2. Dynamical phase diagram for $U = 0$ and corresponding spin trajectories on the Bloch sphere. (a) Dynamical phase diagram for parameters $\omega = 20\text{MHz}$, $\omega_0 = 0.05\text{MHz}$, $\kappa = 8.1\text{MHz}$ taken from Ref. [15], showing the stable attractors of the nonlinear dynamics for $U = 0$. The phases are: \Downarrow all spins down $S_z = -N/2$ and no photons, \Uparrow all spins up $S_z = N/2$ and no photons, a non-trivial magnetised superradiant state with $\psi \neq 0$, and a co-existence region emanating from a tricritical point \bullet . The separatrix $g'/g = \sqrt{\beta_+/\beta_-} = 1.0043$ is close to but distinct from unity. (b) Small cavity loss regime with $\kappa = 1\text{KHz}$ showing the evolution towards the superradiance transition at $g + g' = \sqrt{\omega\omega_0}/N$ in the equilibrium Dicke model [16–19]. The Bloch spheres S1-S4 show the stable \bullet , unstable \circ , and hyperbolic \times fixed points (steady states) as well as characteristic trajectories in each of the phases. Examples of the time evolution for $g = g'$ are given in Fig. 3.

the photon decay rate, $\kappa = 8.1\text{MHz}$, is much greater than the level spacing, $\omega_0 = 0.046\text{MHz}$ [15]. In this limit one obtains a characteristic decay rate for the collective many-body oscillations, $\text{Im}(\nu) = -\kappa\omega_0^2/(\kappa^2 + \omega^2)$, as verified in Fig. 3 (b). Notably, in the limit $\kappa \rightarrow \infty$, corresponding to a *large* cavity loss rate, this results in $\text{Im}(\nu) \rightarrow 0$, or slow decay of the collective oscillations. This may be understood as critical slowing down [25]. Further insight into this $\kappa \rightarrow \infty$ dynamics may be gained by adiabatic elimination of the fast photon field, $\psi = -[i(g + g')S^x + (g - g')S^y]/(\kappa + i\omega)$, to derive an effective equation of motion for the classical spins $\dot{\mathbf{S}} = \{\mathbf{S}, H\} - \Gamma\mathbf{S} \times (\mathbf{S} \times \hat{z})$. Here $H = \omega_0 S_z - \Lambda_+ S_x^2 - \Lambda_- S_y^2$ is the Lipkin–Meshkov–Glick Hamiltonian [26, 27], with $\Lambda_\pm \equiv \frac{\omega}{\kappa^2 + \omega^2}(g \pm g')^2$ and $\Gamma \equiv \frac{2\kappa}{\kappa^2 + \omega^2}(g'^2 - g^2)$. The additional term takes the form of damping in the Landau–Lifshitz–Gilbert equations [28]. Depending on the sign of Γ this favours spin alignment either parallel or anti-

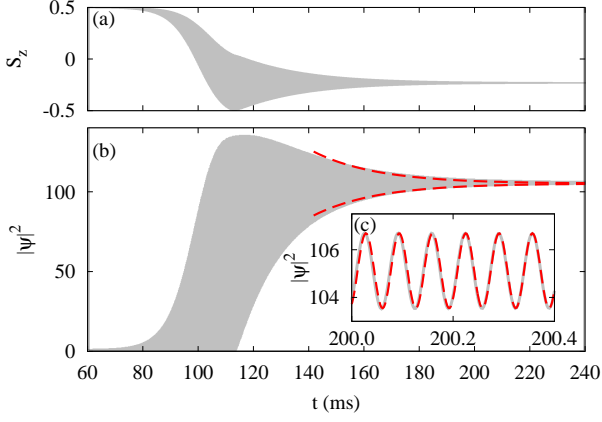


FIG. 3. Time evolution of the effective spin state and cavity photon population. (a) Evolution of S_z and (b) photon number for $g\sqrt{N} = g'\sqrt{N} = 0.791\text{MHz}$ and $U = 0$. The long time behaviour shows the exponential envelope $|\psi|^2 = |\psi_0|^2 \pm \mathcal{A}e^{\text{Im}(\nu)t}$ (dashed lines) where \mathcal{A} is a non-universal amplitude dependant on the initial conditions, and the decay rate $\text{Im}(\nu) = -\kappa\omega_0^2/(\kappa^2 + \omega^2)$. (c) For $\omega_0 \ll \omega$, the long time oscillation frequency is well described by the perturbative result $\text{Re}(\nu) = \omega_0|S|/S_z + \delta$, where $\delta = 4\omega g^2 S_z^2/|S|(\kappa^2 + \omega^2)$ is a small correction to leading term of order ω_0 . The short and intermediate time dynamics can be strongly affected by the existence of additional stable or unstable fixed points.

parallel to the z -axis. The sign change at $g = g'$ is consistent with the $\kappa \rightarrow \infty$ limit of the phase boundary, $g' = g\sqrt{\beta_+/\beta_-}$, which separates the \downarrow and \uparrow steady states. It is interesting to contrast the emergence of integrable dynamics for $g = g'$ and $\kappa \rightarrow \infty$, with the chaotic behaviour when $g = g'$ and $\kappa = 0$ [19]. Moreover, for $g \neq g'$ the dynamics is non-Hamiltonian.

Having discussed the dynamics of the model (1) for $U = 0$, let us now consider $U \neq 0$. In order to make close contact with the experimental realisation in Ref. [15] we henceforth set $g = g'$. In Fig. 4(a) we present the dynamical phase diagram as a function of U . The entire topology may gleaned analytically from the steady state solutions of equation (2). These reveal two classes of superradiant solutions incorporating both U and κ . The first class has a non-vanishing photon population

$$|\psi|^2 = \frac{4g^2}{\tilde{\omega}^2 + \kappa^2} \left(\frac{N^2}{4} - S_z^2 \right), \quad (4)$$

where $\tilde{\omega} \equiv \omega + US_z$, and

$$S_z = -\frac{\omega}{U} \pm \sqrt{\frac{g^2(4\omega^2 - U^2N^2) - U\omega_0\kappa^2}{U^2(\omega_0U + 4g^2)}}, \quad S_y = 0, \quad (5)$$

and S_x is determined by the normalisation of the spins. Physical solutions require $|S_z| \leq N/2$. In the limit $\kappa, U \rightarrow 0$ we recover the results of equilibrium superradiance [16–19], and for $U = 0$ they reduce to those

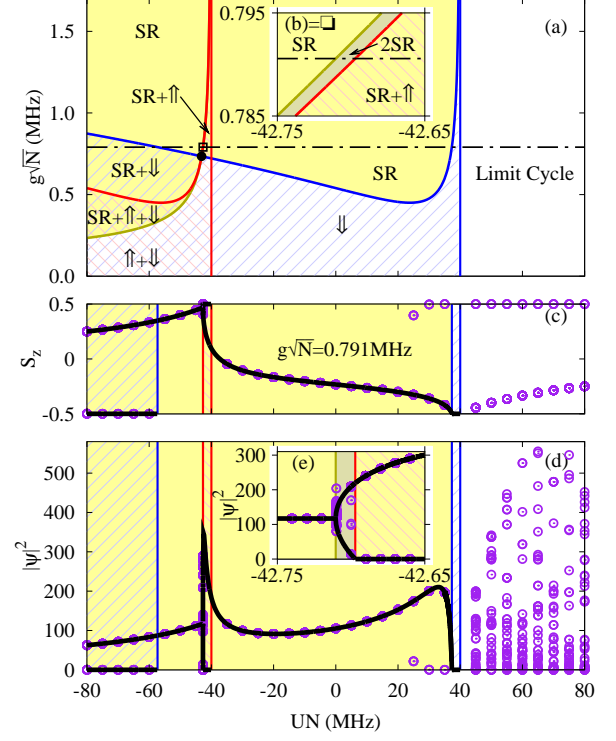


FIG. 4. Dynamical phase diagram as a function of U and long time steady states. (a) Dynamical phase diagram of model (1) with $g = g'$ and parameters $\omega = 20\text{MHz}$, $\omega_0 = 0.05\text{MHz}$, $\kappa = 8.1\text{MHz}$ taken from Ref. [15]. The blue, red and gold critical boundaries correspond to equations (7). (b) Magnified portion showing the appearance of a bistable superradiant phase (2SR) corresponding to co-existence of both roots of equation (5). (c,d) Trajectory along the dashed-dotted line showing the comparison between steady state solutions and numerical integration of the equations of motion at 360ms. The region to the right of the blue asymptote corresponds to a limit cycle. For each value of U we take a variety of initial conditions with $\psi = 1$ and \mathbf{S} uniformly distributed over the Bloch sphere. (e) Magnified portion of the bistable superradiant phase (2SR) showing the agreement between the steady states and numerical integration.

of Ref. [14]. For sufficiently large negative U it is possible for equation (5) to develop unphysical complex roots. In this case one may satisfy equations (2) with $\tilde{\omega}_0 \equiv \omega_0 + U|\psi|^2 = 0$, $\tilde{\omega} \equiv \omega + US_z = 0$, and

$$\psi = i\sqrt{\frac{-\omega_0}{U}}, \quad S_x = -\frac{\kappa}{2g}\sqrt{\frac{-\omega_0}{U}}, \quad S_z = -\frac{\omega}{U}, \quad (6)$$

where S_y is determined by normalisation. Physical solutions have $S_x^2 + S_z^2 \leq N^2/4$. In general these distinct solutions are connected for $g \neq g'$, so we do not distinguish them in Fig. 4(a). Nonetheless, it is important to keep track of them for analytical work when $g = g'$. Figure 4(a) consists of three phase boundaries corresponding to instability of \downarrow (blue), instability of \uparrow (red), and

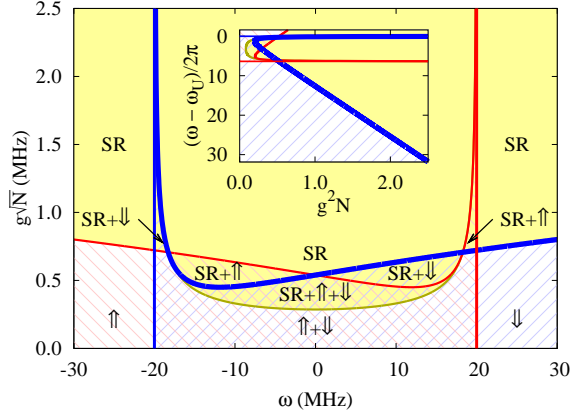


FIG. 5. Dynamical phase diagram as a function of ω for the experimental parameters used in Ref. [15]. Dynamical phase diagram in the $g\sqrt{N}$ versus ω plane for $UN = -40\text{MHz}$, where the blue, red and gold phase boundaries are given by equation (7) and correspond to those in Fig. 4(a). The thick blue line is the boundary of stability of the \downarrow state that would be seen on increasing g as in Ref. [15]. Inset: Phase diagram re-plotted as a function of g^2N for comparison with Fig. 5 of Ref. [15].

existence of the second-type superradiant phase (gold):

$$g_{\downarrow,\uparrow} = \sqrt{\frac{\pm[(\omega \mp \omega_U)^2 + \kappa^2]\omega_0 U}{8\omega_U(\omega \mp \omega_U)}}, \quad g_* = \frac{\kappa}{2} \sqrt{\frac{\omega_0 U}{\omega^2 - \omega_U^2}}, \quad (7)$$

where $\omega_U \equiv UN/2$. Instability of the normal state g_{\downarrow} has also been considered for thermal clouds in a ring cavity [9]. The result for g_* delimits the region, both for equation (5) and equation (6), to have real, physical solutions. All three of these boundaries intersect at $U = -2N^{-1}\sqrt{\omega^2 + \kappa^2}$, $g = \sqrt{-\omega_0 U/4}$, as shown in Fig. 4(a). Upon increasing g one finds a phase where two distinct first-type superradiant solutions co-exist; see Fig. 4(b). This is borne out in Fig. 4(c,d,e), where we compare the steady states with direct integration of equations (2) along the dashed-dotted line in Fig. 4(a). We integrate over a period of 360 ms to eliminate the transitory effects of critical slowing down discussed earlier. In addition, Fig. 4 contains several regions involving co-existence of superradiant *and* non-superradiant phases.

The scattered points in Fig. 4(d), beyond the \downarrow boundary at $U = 2\omega/N$, correspond to limit cycles rather than steady states. Here $S_z = -\omega/U$ and ψ is purely imaginary. Writing $S^- = re^{-i\theta}$, where $r = \sqrt{N^2/4 - \omega^2/U^2}$, yields $\partial_t \theta = \omega_0 + U|\psi|^2$, and $(\partial_t + \kappa)\psi = -2igr \cos(\theta)$, with limit cycle behaviour. For $\kappa \gg \omega_0 + U|\psi|^2$, these describe a damped driven pendulum.

Having confirmed the overall phase diagram in Fig. 4(a) as a function of U , let us finally focus on the specific value $UN = -40\text{MHz}$ used in Ref. [15]. In Fig. 5 we plot the phase diagram as a function of ω for this fixed

value of U . We see that the superradiance boundary is accompanied by several regions of multi-phase co-existence. It would be extremely interesting to investigate this experimentally. The inset shows the same data shifted and rescaled for comparison with Fig. 5 of Ref. [15].

In summary, we have discussed the collective dynamics of BECs in optical cavities. We obtain a rich phase diagram with different regimes of dynamical behaviour, including several regions of multi-phase co-existence and the slow decay of many-body oscillations. Amongst our findings is a regime of persistent optomechanical oscillations described by a damped driven pendulum. Given the strong interest in cavity optomechanics [5, 6] this may be a profitable region to explore experimentally. Further directions include the impact of cavity axis pumping [29] and photon correlations. Experiments in which the coupling g is quenched through the phase boundaries may help explore this rich dynamics.

We are extremely grateful to K. Baumann, F. Brennecke, T. Esslinger and M. Köhl for illuminating discussions. MJB and JK acknowledge ETH Zürich, G. Blatter, S. Schmidt, and H. Türeci for hospitality and interactions. MJB and BDS acknowledge EPSRC grant no. EP/E018130/1. JK acknowledges EPSRC grant no. EP/G004714/1.

-
- [1] F. Brennecke, T. Donner, S. Ritter, T. Bourdel, M. Köhl, and T. Esslinger, *Nature* **450**, 268 (2007).
 - [2] Y. Colombe, T. Steinmetz, G. Dubois, F. Linke, D. Hunger, and J. Reichel, *Nature* **450**, 272 (2007).
 - [3] I. B. Mekhov, C. Maschler, and H. Ritsch, *Nat. Phys.* **3**, 319 (2007).
 - [4] W. Chen, D. Meiser, and P. Meystre, *Phys. Rev. A* **75**, 023812 (2007).
 - [5] F. Brennecke, S. Ritter, T. Donner, and T. Esslinger, *Science* **322**, 235 (2008).
 - [6] S. Ritter, F. Brennecke, K. Baumann, T. Donner, C. Guerlin, and T. Esslinger, *Appl. Phys. B* **95**, 213 (2009).
 - [7] P. Domokos and H. Ritsch, *Phys. Rev. Lett.* **89**, 253003 (2002).
 - [8] A. T. Black, H. W. Chan, and V. Vuletić, *Phys. Rev. Lett.* **91**, 203001 (2003).
 - [9] D. Nagy, J. K. Asbóth, P. Domokos, and H. Ritsch, *Europhys. Lett.* **74**, 254 (2006).
 - [10] D. Nagy, G. Szirmai, and P. Domokos, *Eur. Phys. J. D* **48**, 127 (2008).
 - [11] J. Larson, B. Damski, G. Morigi, and M. Lewenstein, *Phys. Rev. Lett.* **100**, 050401 (2008).
 - [12] J. Larson, S. Fernández-Vidal, G. Morigi, and M. Lewenstein, *New J. Phys.* **10**, 045002 (2008).
 - [13] S. Gopalakrishnan, B. L. Lev, and P. M. Goldbart, *Nat. Phys.* **5**, 845 (2009).
 - [14] F. Dimer, B. Estienne, A. S. Parkins, and H. J. Carmichael, *Phys. Rev. A* **75**, 013804 (2007).
 - [15] K. Baumann, C. Guerlin, F. Brennecke, and T. Esslinger, *arXiv:0912.3261*.

- [16] R. H. Dicke, Phys. Rev. **93**, 99 (1954).
- [17] K. Hepp and E. H. Lieb, Ann. Phys. **76**, 360 (1973).
- [18] Y. K. Wang and F. T. Hioe, Phys. Rev. A **7**, 831 (1973).
- [19] C. Emary and T. Brandes, Phys. Rev. E **67**, 066203 (2003).
- [20] D. Nagy, G. Konya, G. Szirmai, and P. Domokos, arXiv:0912.3260.
- [21] A. V. Andreev, V. Gurarie, and L. Radzihovsky, Phys. Rev. Lett. **93**, 130402 (2004); R. A. Barankov and L. S. Levitov, *ibid.* **93**, 130403 (2004).
- [22] P. R. Eastham, J. Phys. Condens. Matter **19**, 295210 (2007); P. R. Eastham, M. H. Szymanska, and P. B. Littlewood, Solid State Commun. **127**, 117 (2003).
- [23] G. Szirmai, D. Nagy, and P. Domokos, arXiv:1001.1818.
- [24] For $\kappa = 0$, we recover Dicke model superradiance at $g + g' = \sqrt{\omega\omega_0/N}$. For $g = g'$ it yields the results of Ref. [14]. See also Ref. [9].
- [25] P. C. Hohenberg and B. I. Halperin, Rev. Mod. Phys. **49**, 435 (1977).
- [26] H. J. Lipkin, N. Meshkov, and A. J. Glick, Nucl. Phys. **62**, 188 (1965); N. Meshkov, A. J. Glick, and H. J. Lipkin, *ibid.* **62**, 199 (1965); A. J. Glick, H. J. Lipkin, and N. Meshkov, *ibid.* **62**, 211 (1965).
- [27] S. Morrison and A. S. Parkins, Phys. Rev. A **77**, 043810 (2008).
- [28] L. D. Landau and E. M. Lifshitz, Phys. Z. Sowjet. **8**, 153 (1935); T. L. Gilbert, IEEE Trans. Mag. **40**, 3443 (2004).
- [29] A. Tomadin, V. Giovannetti, R. Fazio, D. Gerace, I. Carusotto, H. E. Tureci, and A. Imamoglu, arXiv:0904.4437.